Phys Chem Minerals (2003) 30: 495–502
DOI 10.1007/s00269-003-0357-8

ORIGINAL PAPER

S. C. Tarantino · M. A. Carpenter
M. C. Domeneghetti

Strain and local heterogeneity in the forsterite–fayalite solid solution

Received: 28 October 2002 / Accepted: 14 January 2003

Abstract Infrared powder-absorption spectra of nine natural and five synthetic olivine samples across the forsterite–fayalite join have been investigated at room temperature in the range 70–1400 cm^{-1}. Variations of peak positions as a function of Fe content are close to linear for those vibrational bands whose trend could be followed across the solid solution. Line-broadening has been quantified by autocorrelation analysis. Positive deviations from linearity of the line-broadening parameter, Δ_{corr}, for groups of bands at low energies are consistent with the existence of local elastic strain heterogeneities at intermediate compositions in the solid solution. It also appears that the structure of forsterite is more homogeneous than Fe-rich olivines in relation to local elastic strain effects. Positive deviations from linearity of the line-broadening parameter for the low-energy regions scale linearly with calorimetric data for the enthalpy of mixing. This close correlation between line-broadening in IR spectra and calorimetric enthalpies of mixing has now been observed for four different binary solid solutions, and there is a further, qualitative correlation with bulk modulus.

Keywords Olivine · Solid solution · IR spectroscopy · Line-broadening · Elastic strain

Introduction

The forsterite–fayalite solid solution has received considerable attention in mineral physics and petrological studies because of the frequent occurrence of olivine in crustal rocks and its importance as a constituent phase of the upper mantle. One focus has been on the thermodynamic mixing properties. Partitioning of Fe and Mg between olivine and other ferromagnesian minerals has been used to evaluate thermodynamic properties of the coexisting minerals and to establish geobarometers and geothermometers (e.g. O'Neill and Wood 1979; Kawasaki and Matsui 1983; Wiser and Wood 1991; von Seckendorff and O'Neill 1993). More direct determinations of Fe–Mg mixing properties are based on enthalpies of solution measurements made by Wood and Kleppa (1981) and more recently by Kojitani and Akaogi (1994). A small positive deviation from ideality has been found. Ordering of Mg and Fe^{2+} between M1 and M2 sites in natural and synthetic samples tends to be rather limited in extent (Artioli et al. 1995; Redfern et al. 2000; Rinaldi et al. 2000).

The intention of the present paper is to describe an alternative approach for analyzing mixing behaviour at a microscopic length scale, using the properties of IR spectra. The underlying hypothesis is that non-ideal mixing of silicate solid solutions can be understood in terms of local strain heterogeneities arising from the replacement of one cation by another. There is, as yet, no determination of the length scale of a structure sampled in hard-mode infrared spectroscopy experiments, but it seems likely that phonon spectra contain information from the length scale of interest in the context of local strain and solid-solution formation. Recent experience has shown that peak shifts and linewidth variations of phonon spectra can be used to detect the structural response to any local change associated with mixing and ordering (Boffa Ballaran et al. 1998, 1999; Atkinson et al. 1999; Carpenter and Boffa Ballaran 2001; Tarantino et al. 2002). Particular attention will be paid to line-broadening, which can be quantified by the autocorrelation method (Salje et al. 2000) and interpreted as being indicative of local elastic strain fields.

S. C. Tarantino (✉) · M. C. Domeneghetti
Dipartimento di Scienze della Terra,
Università di Pavia, via Ferrata 1, 27100 Pavia, Italy
Tel: +39-0382-505842
Fax: +39-0382-505890
e-mail: tarantino@crystal.unipv.it

M. A. Carpenter
Department of Earth Sciences,
University of Cambridge, Downing St.,
Cambridge, CB2 3EQ, UK

From many studies it is known that elastic strain is an important, if not dominant, factor in determining the thermodynamic behaviour of phase transitions, mixing and ordering processes (e.g. Christian 1975; Greenwood 1979; Newton and Wood 1980; Davies and Navrotsky 1983; for a recent review see Geiger 2001 and references therein). Recently, it has been argued that the important part of the strain, in energy terms, is in fact associated with local structural heterogeneities (Boffa Ballaran et al. 1998; Atkinson et al. 1999; Tarantino et al. 2002; Carpenter 2003). Substituting a smaller cation for a larger one would create a local strain field as the matrix deforms to accommodate the change in size. Associated with such a strain field will be a positive elastic energy, depending on the elastic constants of the host crystal. From this point of view, a solid solution would be expected to develop a positive excess enthalpy of mixing unless the atoms are similar in size and charge to those they are replacing.

Experimental methods

Samples

Nine natural, homogeneous olivine samples with low contents of minor elements were chosen to cover a wide range of Fe/(Fe + Mg). A brief description of the analyzed samples is given in Table 1. Powders of Mg_2SiO_4 (Fo_{100}) and Fe_2SiO_4 (Fa_{100}) were synthesized in evacuated silica tubes at 950 °C using Ni/NiO as oxygen buffer. Commercial MgO, Fe_2O_3, Fe and SiO_2 were used as starting materials. Powders of synthetic Fo30, Fo50 and Fo75 samples were kindly provided by Professor H. Kroll.

Microprobe analysis

Compositions were determined by electron microprobe analysis (CAMECA SX50), operating at 20 kV with a 15-nA sample current. All elements were determined by energy-dispersive analysis using a Link AN10000 system with ZAFS/FSL quantitative software. Up to 20 point analyses were obtained from several crystals of each sample. The average compositions are reported in Table 2. They are expressed in terms of X_{Fo}, which is the mole fraction of forsterite.

X-ray diffraction

Unit-cell parameters from natural samples, reported in Table 3, were obtained on a Philips PW1100 four-circle automated diffractometer with graphite monochromatized Mo$K\alpha$ radiation ($\lambda = 0.71073$ Å), using least-squares methods, based on a locally improved version (Cannillo et al. 1983) of the Philips LAT routine. This takes into account 50 to 60 d^* spacings, each measured by considering all the reflections in the range $3° < \theta < 25°$.

The suite of five synthetic olivines was characterized by X-ray powder diffraction, using a Philips 1710 diffractometer equipped with a copper anode operating at 40 kV and 35 mA, a graphite curved monochromator on the diffracted beam and a proportional counter. Unit-cell parameters, reported in Table 3, were determined by minimizing the weighted squared difference between calculated (using data of Boström 1987) and experimental Q_i values, where $Q_i = 4\sin^2\theta_i/\lambda_i$ and weight $= \sin(2\theta_i)^2$. Instrumental aberrations were considered by inserting additional terms into the linear least squares.

IR spectroscopy

Pellets for IR powder absorption spectroscopy were prepared following the procedure described by Zhang et al. (1996). Two types of pellets were prepared under vacuum and used for the different energy ranges. Pellets of polyethylene, weighing 100 mg with a sample:matrix ratio of 1:50, were used for the spectral region 50–650 cm^{-1} (FIR). Pellets of CsI, weighing 300 mg with a sample:matrix ratio of 1:250, were used for the spectral region 400–4000 cm^{-1} (MIR).

Spectra were recorded under vacuum at room temperature with a resolution of 2 cm^{-1}, using a Bruker 113 V FT-IR spectrometer for the FIR region and a Bruker 66 V FT-IR spectrometer for the MIR region. Spectra of the same samples recorded on both instruments showed no measurable differences. Every spectrum, recorded as absorbance using a DTGS detector, was calculated by Fourier transformation of 512 interferometer scans. Spectra measured using polyethylene and CsI pellets were merged using the software OPUS/IR (Bruker analytische Messtechnik GmbH) by matching up far- and mid-IR sections in the regions 400–500 cm^{-1}, where they overlap. All quantitative analysis was performed on the original unmerged spectra.

Results and discussion

X-ray diffraction

The variation in lattice parameters with composition across the forsterite–fayalite join is shown in Fig. 1. A slightly non-linear variation of unit-cell volume as a function of Fo content is evident within the resolution of our measurements. There is good agreement between the powder diffraction data from the synthetic samples

Table 1 Rock and mineral types, and locality for the investigated natural samples

Sample	Rock or mineral name	Locality
Le8	Spinel-lherzolite xenolith	M.Leura, Victoria, Australia
Ka111[a]	peridotitic xenolith	Kapfestein, Austria
120651[b]	Dunite	unknown
120644[b]	Dunite	unknown
PU8[c]	Volcanic sand	Stromboli, Italy
Ska 9005	Orthopyroxenite, Skaergard ultramafic complex	Skaergard, Greenland
99.37.1[d]	Hortonolite	O'Neil Mine, Monroe Co., New York, USA
8575[b]	Eulite	madial sheet 86 C, Sudan
34950[b]	Eulite	Mansjö, Loos, Sweden

[a]Kindly provided by R. Vannucci
[b]Mineral collection Dept. of Earth Sciences Cambridge
[c]Kindly provided by F. Caucia
[d]Kindly provided by C. Francis, Harvard Mineralogical Museum

Table 2 Electron microprobe analyses (standard deviations are *in parentheses*)

	le8	ka111	12651	PU8	120644	Ska9005	99.37.1	8575	34950
SiO_2	40.7(1)	40.2(3)	38.9(4)	37.8(1)	36.4(4)	35.7(5)	32.2(1)	29.7(1)	29.1(1)
FeO	8.8(1)	9.93(8)	19.4(2)	25.7(4)	33.1(3)	37.5(3)	53.3(3)	68.5(3)	69.0(2)
MnO	0.11(3)	0.15(4)	0.29(5)	0.53(4)	0.57(4)	0.53(4)	3.00(7)	0.59(4)	0.5(6)
MgO	50.1(1)	49.0(4)	41.4(2)	36.1(3)	30.2(4)	26.5(2)	12.3(2)	1.8(1)	1.6(1)
CaO	0	0.06(3)	0	0.33(3)	0.0	0.08(2)	0	0	0
NiO	0.39(5)	0.35(4)	0.16(4)	0	0	0.07(4)	0	0	0
Oxide total	100.1(2)	99.6(5)	100.15	100.1(2)	100.2(7)	100.4(6)	100.8(3)	100.6(3)	100.2(3)
Si	0.994(2)	0.994(6)	0.997(4)	0.996(2)	0.996(3)	0.999(7)	0.993(2)	0.99(2)	0.981(3)
Fe^{2+}	0.178(2)	0.204(2)	0.415(6)	0.56(1)	0.76(1)	0.88(1)	1.372(6)	1.911(6)	1.944(8)
Mn	0.0024(7)	0.003(1)	0.006(1)	0.011(1)	0.013(1)	0.012467	0.078(2)	0.017(2)	0.014(2)
Mg	1.822(3)	1.80(1)	1.581(9)	1.42(1)	1.235(8)	1.11(1)	0.563(6)	0.088(5)	0.080(6)
Ca	0	0.001(1)	0	0.009(1)	0	0.002(1)	0	0	0
Ni	0.008(1)	0.007(1)	0.0030(8)	0	0	0.002(1)	0	0	0
	3.006(2)	3.004(6)	3.002(2)	3.004(2)	3.004(3)	3.001(7)	3.007(2)	3.009(2)	3.019(3)
Forsterite	91.0(1)	89.6(2)	79.0(3)	71.1(5)	61.6(4)	55.4(4)	28.0(3)	4.3(3)	3.9(3)
Fayalite	8.9(1)	10.2(1)	20.7(2)	28.3(5)	37.8(4)	44.0(4)	68.2(3)	94.8(3)	95.4(3)
Tephroite	0.11(3)	0.15(5)	0.31(5)	0.59(4)	0.66(4)	0.63(4)	3.8(1)	0.83(5)	0.70(8)

Table 3 Unit-cell parameters of the studied natural and synthetic olivines

Samples	*a* (Å)	*b* (Å)	*c* (Å)	V ($Å^3$)
Natural				
val	4.763(2)	10.226(3)	5.994(2)	291.9(2)
ka111	4.763(3)	10.228(5)	5.993(5)	292.0(4)
120651	4.770(1)	10.257(3)	6.007(1)	293.9(1)
pu8	4.778(3)	10.286(5)	6.014(3)	295.5(4)
120644	4.782(2)	10.306(3)	6.028(2)	297.1(2)
ska 9005	4.785(2)	10.319(2)	6.029(2)	297.7(2)
99.37.1	4.807(1)	10.410(3)	6.064(2)	303.4(1)
8575	4.816(2)	10.463(4)	6.082(2)	306.5(2)
34950	4.818(3)	10.465(4)	6.085(3)	306.8(3)
Synthetic				
Fo100	4.750(2)	10.197(4)	5.980(2)	289.6(2)
Fo75	4.765(2)	10.240(3)	5.999(3)	292.7(2)
Fo50	4.790(1)	10.337(3)	6.037(4)	298.9(2)
Fo30	4.804(2)	10.390(4)	6.056(2)	302.3(2)
Fa100	4.821(2)	10.474(5)	6.090(3)	307.5(2)

and the single-crystal diffraction data from the set of natural samples, although the latter are more scattered. The following regressions were calculated using data from the synthetic samples. The unit-cell volume is described by: $V(\text{cell}) = 307.5(7) - 16.6(7) \cdot X_{\text{Fo}} - 1.1(7) \cdot X_{Fo}{}^2 (Å^3)$. The non-linear variation in volume may be ascribed mainly to the variation of the *a* unit-cell parameter with composition. It is evident from Fig. 1 that, although the *b*- and *c*-cell edges vary linearly with composition, the *a*-cell edge shows a small positive excess. Unweighted regressions of the data yield the following relationships Å

$$a = 4.821(1) - 0.506(5)X_{\text{Fo}} - 0.020(2)X_{\text{Fo}}^2 : (\text{Å})$$

$$b = 10.474(1) - 0.00276(1)X_{\text{Fo}}(\text{Å})$$

$$c = 6.091(1) - 1.08(2)X_{\text{Fo}}(\text{Å}).$$

These data are in agreement with those of Schwab and Küstner (1977), within the uncertainties of both sets of measurements.

IR spectroscopy

IR spectra for the high- and low-energy regions from the natural and synthetic olivine samples are shown in Fig. 2. Olivine end members are expected to show 35 IR-active modes by factor group analysis (for a detailed analysis see McMillan 1985). Only about 12 peaks can be discerned in the recorded spectra, although some are rather broad.

Assignment of the active modes of the olivine end-member spectra has been considered in detail by many authors (e.g. Hofmeister 1987, 1997; Chopelas 1991; for a recent review see Geiger and Kolesov 2003 and references therein). This is not of primary interest in the present study, however. The high-energy modes involve motions within the SiO_4 tetrahedra. The low-energy vibrations are lattice modes, which involve motions of all atoms in the structure. There are many overlapping peaks, but variations with composition are evident as changes in frequency and linewidth.

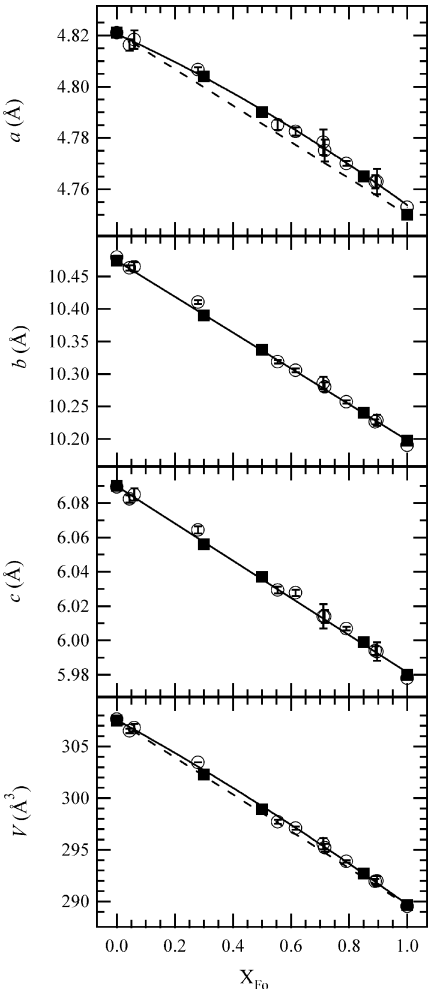

Fig. 1a–d Variation in unit-cell parameters of olivine as a function of composition on the join Mg_2SiO_4–Fe_2SiO_4. *Open circles* Natural samples; *solid squares* synthetic samples

The low-energy region is shown in greater detail in Fig. 3. The end members show very different features at these low wavenumbers, and broadening of all the absorption bands is apparent for the intermediate compositions.

Wavenumber shifts

Individual phonon bands can be followed across the solid solution at high energies, but at low energies, changes in absorbance and peak position are not as easy to follow. The wavenumber variations of selected peaks, as numbered in Fig. 2, were obtained using a computer routine that identifies peak maxima by analyzing first and second derivatives of the absorption signals. Their wavenumber variations are shown in Fig. 4. The few unambiguous trends, traced across above 400 cm^{-1}, appear to be linear. Shifts of peak 7 as a function of X_{Fo} show a perhaps slight negative deviation from linearity. The pattern of wavenumber variations of peaks 8 and 9 is different, however. Peaks 8a and 8b appear to diverge

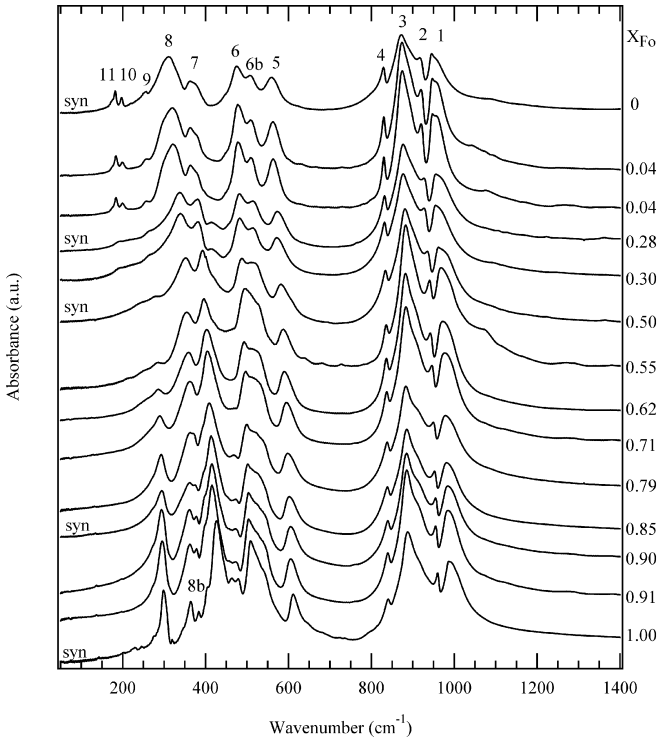

Fig. 2 Infrared powder absorption spectra at room temperature of natural and synthetic olivines. Composition is expressed as X_{Fo}. Spectra from synthetic samples are labelled syn

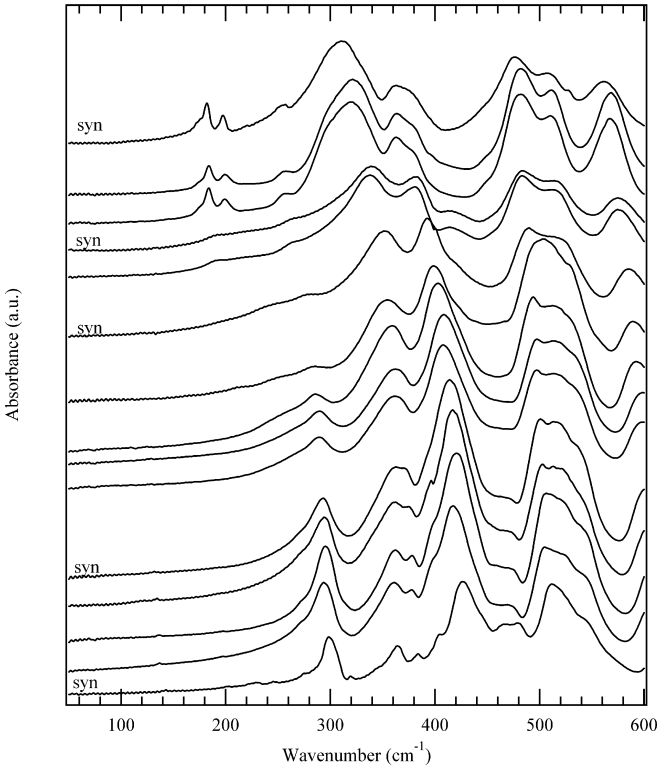

Fig. 3 IR powder absorption spectra in the far-IR range

at Mg-rich compositions (Fig. 4d). The wavenumber of peak 9 varies linearly as a function of composition across about half of the solid solution, but has a displacement and change of slope at Fo_{40}. Furthermore, the intensity of this peak decreases as forsterite content increases, approaching zero near the middle of the binary. This could suggest two-mode behaviour that, as has been suggested before, might be expected at low frequencies (Hofmeister et al. 1996; Hofmeister 1997 and references therein). In the limiting case of this behaviour, the spectrum of an intermediate member of a solid solution should be similar to the superposition of the IR spectra of the two end members. In order to test this model, a spectrum, obtained by combining spectra of the end members in the proportion 50:50, was compared with the spectra from sample Fo_{50}. It is evident from Fig. 5 that the combined spectrum is substantially different from the experimental spectrum of the synthetic sample in both the high- and low-energy ranges. Wavenumber shifts and broadening of vibrational bands at intermediate compositions result from local structural changes and not from the simple superposition of absorption by phonons in "forsterite-like" and "fayalite-like" regions.

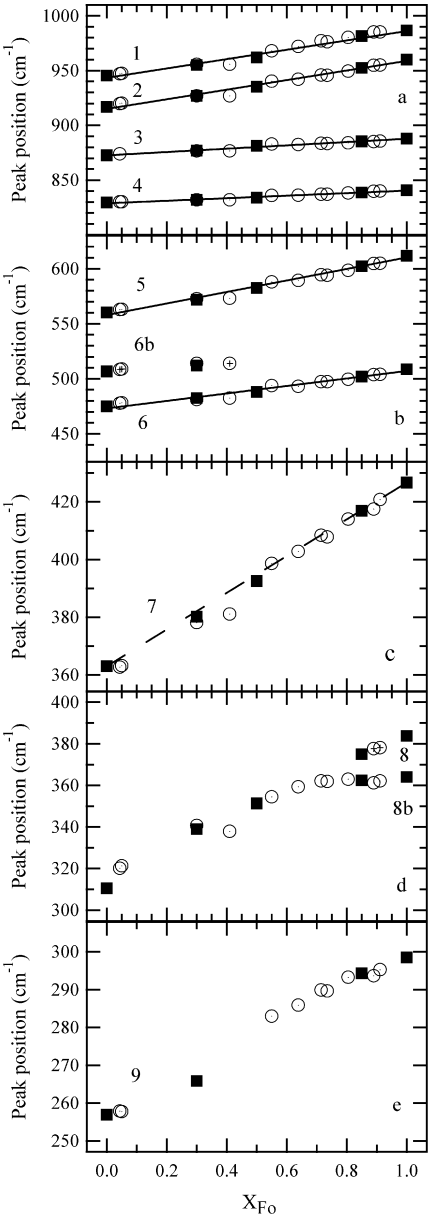

Fig. 4a–d Wavenumber shifts of the modes numbered in Fig. 2 as a function of composition across the join Mg_2SiO_4–Fe_2SiO_4. *Symbols* as in Fig. 1. *Solid lines* are the regression equations through the synthetic set of data; *dashed line* is a linear interpolation between the two end members

Line broadening and Fe/Mg mixing

In the past few years, a systematic methodology of sample grinding and pellet preparation has been developed for generating reproducible results in IR powder absorption spectroscopy studies (Zhang et al. 1996). This has allowed, in particular, detailed examination of variations in linewidths due to the effects of composition and cation order across mineral solid solutions. The autocorrelation method (Salje et al. 2000) has been used to determine effective linewidth (Δ_{corr}) variations of phonon bands in a given spectral interval. The critical point for applying this method successfully lies in the choice of which wavenumber region to analyze. The chosen spectral segment may contain single peaks or groups of peaks, but the limits of each segment must lie on a single and well-defined baseline.

Three spectral ranges were chosen for the calculation of Δ_{corr}: 711–1400 cm^{-1}; 590/635–636/690 cm^{-1}; 70/100–433/460 cm^{-1}. In order to subtract a reasonable baseline and to analyze the same group of peaks, the spectral limits of the latter two analyzed regions were adjusted as a function of composition, but with the number of data points kept constant in each case. A polynomial baseline was subtracted. In the low-energy region, Δ_{corr} values for the fayalites were calculated after the removal of peaks 10 and 11 from the analyzed spectral region. These peaks occur only in spectra from Fa-rich olivines and are substantially sharper than the

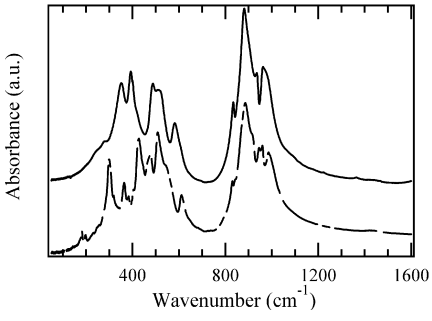

Fig. 5 Comparison between the observed spectrum from the sample Fo_{50} (*solid line*) and the spectrum obtained by combining spectra from the end members in the proportion 50:50 (*broken line*)

others. Their inclusion would introduce a bias into comparisons of line-broadening of the 200–700 cm^{-1} group of absorption bands. The variations of effective linewidth are shown as a function of composition in Fig. 6. Fig. 6c shows Δ_{corr} values for the low-energy region with and without the inclusion of peaks 10 and 11.

Interpretation of line-broadening in olivine spectra using the autocorrelation method must be approached with some caution because of the large wavenumber shifts that give rise to peak merging. This is particularly evident in Fig. 2 for the region above 800 cm^{-1}. The absorption bands are related to stretching motions within the SiO_4 tetrahedra (Lazarev 1972) and their frequencies change systematically with composition. Wavenumber variations of some bands are steeper than others, as is evident in Fig. 4a, and the degree of overlap also changes, therefore. The variation of Δ_{corr} as a function of composition in this region is shown in Fig. 6a. Apart from the data for Fa-rich samples, Δ_{corr} does not change significantly across the solid solution. The apparently sharper bands in spectra from fayalites could be due simply to increased overlap of bands, which diverge with increasing Fo content.

In the other two analyzed regions, some peak merging also occurs, but the dominant changes are in the broadening of a very few large peaks. A more reproducible pattern of Δ_{corr} with composition is observed, although Δ_{corr} data from the natural samples, characterized by slightly different degrees of order and impurities, are slightly more scattered. In these regions a "positive excess" type of variation is found and the only real difference between spectral regions is the absolute value of the "excesses", $\delta\Delta_{corr}$, relative to a straight line connecting the end-member values of Δ_{corr}. It is worth noting that, at wavenumbers below 800 cm^{-1}, inspection of the primary spectra is sufficient to indicate that the spectrum of pure Fa has broader absorption bands than those of pure Fo. If interpreted in terms of local heterogeneity this observation implies that there are considerable distortions when both M1 and M2 sites are filled by Fe, in comparison with when they are both filled by Mg. Furthermore, even a small amount of Fe substituted for Mg is sufficient to increase the line width of the IR modes, as is particularly evident in Fig. 3 for low-energy modes. Hardly any change in line-broadening appears to be evident at the fayalite end when small amounts of Mg are substituted for Fe. If it is assumed that positive enthalpies of mixing are mainly due to local elastic strain energies caused by cation substitution in a heterogeneous sample, it should be expected that line-broadening, as measured by the autocorrelation analysis, will be a good proxy for these enthalpies. The positive deviation from linearity observed in the low-energy regions for Δ_{corr} values is taken as being indicative of local heterogeneity, which could contribute to a positive enthalpy of mixing, ΔH_{mix}. This contribution seems to be symmetric with respect to $Fo_{50}Fa_{50}$, as is evident from Fig. 7 which shows an "excess" in $\Delta_{corr,150}$, $\delta\Delta_{corr,150}$, taken as the deviation from linearity of the curve through the data for the synthetic series of samples. The synthetic samples are expected to give a more consistent picture of the mixing behaviour in this context. This is because, as pointed out above, they seem to be more homogeneous with respect to degree of order and level of impurities. A symmetrical variation of $\delta\Delta_{corr,150}$ is in agreement with the calorimetric data of Kojitani and Akaogi (1994). In Fig. 7, $\delta\Delta_{corr,150}$ has been plotted on the same graph as ΔH_{mix} from Kojitani

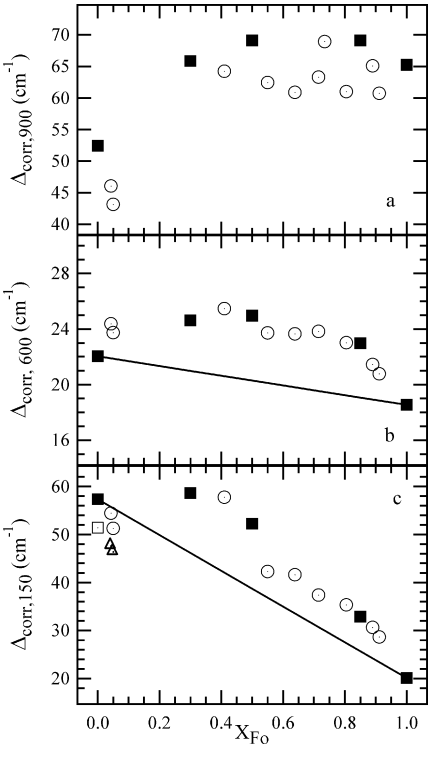

Fig. 6a–c Variation with composition of Δ_{corr} values calculated in the regions. **a** 711–1400 cm^{-1}, $\Delta_{corr,900}$ **b** 590/635–636/690 cm^{-1}, Δ_{corr} **c** 70/100–433/460 cm^{-1}, $\Delta_{corr,150}$. *Symbols* as in Fig. 1. *Open square* and *triangles* refer to Δ_{corr} values for the fayalites before the removal of peaks 10 and 11 from the analyzed spectral region

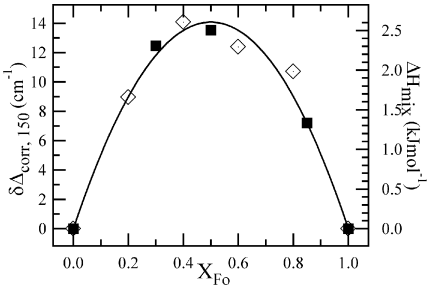

Fig. 7 Variation with composition of the excess line broadening of IR absorption peaks in the low-energy region ($\delta\Delta_{corr,150}$, *solid squares*) and enthalpy of mixing (ΔH_{mix}, *open diamonds*) for the forsterite–fayalite solid solution. Calorimetric enthalpy of mixing data are from Kojitani and Akaogi 1994. *Solid line* represents the fit through the $\delta\Delta_{corr,150}$ data reported in the text

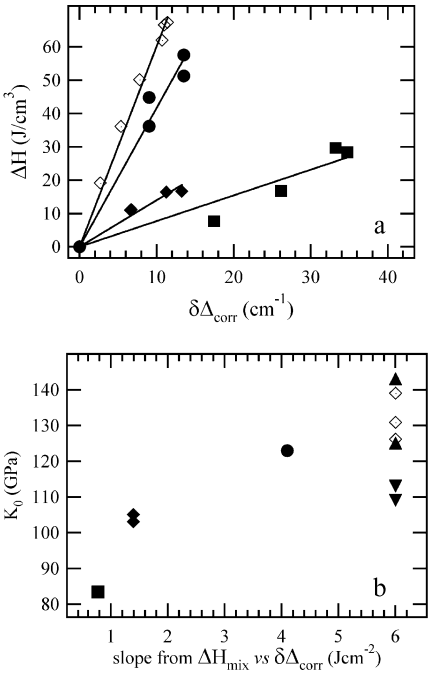

Fig. 8a Correlation between enthalpy data and $\delta\Delta_{corr}$ values for different silicate solid solutions. *Open diamonds* Augite–jadeite; *filled squares* $I\bar{1}$ and $P\bar{1}$ plagioclase feldspars; *filled diamonds* enstatite–ferrosilite, *solid circles* forsterite-fayalite. **b** Qualitative correlation between the slopes of the lines in **a** and bulk modulus, K_0, values from the literature. *Filled upward-pointing triangles* diopside from Levien and Prewitt (1981) and Zhao et al. (1998); *filled downward-pointing triangles* jadeite from Kandelin and Weidner (1979) and Zhao et al. (1997); *open diamonds* omphacites from Bhagatt et al. (1992), McCormick et al. 1989 and Nishihara et al. (2003); *solid circle* forsterite from Kudoh and Takeuchi (1985); *solid square* anorthite from Hackwell and Angel 1992; *solid diamonds* orthoenstatite from Angel and Hugh–Jones (1994), Jackson et al. (1999) and Angel and Jackson (2002)

and Akaogi (1994). There is, as yet, no theoretical model to equate ΔH_{mix} with Δ_{corr} directly, but the overlap of the data is remarkable. It is possible to fit the $\delta\Delta_{corr,150}$ data with a symmetric expression analogous to the form used for a regular solution model: $\delta\Delta_{corr} = 2aX_{Fo}(1 - X_{Fo})$ with $a = 28.2\,cm^{-1}$.

An empirical calibration of $\delta\Delta_{corr,150}$ in terms of ΔH_{mix} has been achieved using the calorimetric data of Kojitani and Akaogi (1994). The interaction parameter, obtained using the empirical calibration and expressed now in kJ mol^{-1}, is $a = 5.3\,kJ\,mol^{-1}$. This value is similar to the calorimetric interaction parameter, $a = 5.3(1.7)$ kJ mol^{-1} from Kojitani and Akaogi (1994), and to $a = 6.3(2.5)$ kJ mol^{-1} from Wood and Kleppa (1981) ignoring asymmetry.

In Fig. 8a, the correlation between enthalpy of mixing and $\delta\Delta_{corr,150}$ for the olivine solid solution is compared with equivalent data for Fe–Mg orthopyroxene (Tarantino et al. 2002), jadeite–augite (Boffa Ballaran et al. 1998) and albite–anorthite (Atkinson et al. 1999) solid solutions. Values of enthalpy were normalized with respect to molar volumes rather than with respect to formula units, for the purpose of this comparison. The correlation is reasonably linear for all the analyzed solid solutions. The proportionality constant might be a function of the difference in size and charge of the exchanged cations and of the "accommodatability" of the structure. A rough measure of the accommodatability, in the present context, might be provided by some bulk elastic property such as the bulk modulus. A correlation between bulk modulus, K_0, and the slopes of the empirical calibrations in Fig. 8a would then support the suggestion of the overall mixing behaviour being determined by elastic effects. This correlation is shown in Fig. 8b. In spite of the scatter of K_0 data for clinopyroxenes, there is a general increase of $\delta\Delta_{corr}/\Delta H_{mix}$ with decreasing compressibility of the structure. In other words, elastically soft materials have a larger energy change per unit of line-broadening in IR spectra than those which are elastically stiff. These empirical correlations between line-broadening, excess enthalpy and elastic effects reinforce the view that:

1. Exchange of atoms onto different crystallographic sites causes structural relaxation which can lead to heterogeneous strain fields, the dimensions of which exceed the next-neighbour spacings.
2. Local elastic strain fields could be responsible for a substantial part of the excess enthalpy of mixing or enthalpy of ordering in silicate systems.

Acknowledgements The authors thank Dr. C. Francis, Harvard Mineralogical Museum, Prof. F. Caucia and Prof. R. Vannucci for providing natural samples. Prof. H. Kroll is thanked for kindly donating synthetic Fo30, Fo50 and Fo75 samples. Critical review by C.A. Geiger helped to improve the manuscript. Dr. M. Zhang provided invaluable assistance for the IR experiments. Dr. S. Reed is thanked for microprobe analyses. Financial support was provided by the Italian MURST Cofin Project 2001 Structural evolution and phase transition in minerals vs. temperature, pressure and composition.

References

Angel RJ, Hugh-Jones DA (1994) Equation of state and thermodynamic properties of enstatite pyroxenes. J Geophys Res 99: 19777–19783

Angel RJ, Jackson JM (2002) Elasticity and equation of state of orthoenstatite, $MgSiO_3$. Am Mineral 87: 558–561

Atkinson AJ, Carpenter MA, Salje EKH (1999) Hard-mode infrared spectroscopy of plagioclase feldspars. Eur J Mineral 11: 7–21

Artioli G, Rinaldi R, Wilson CC, Zanazzi PF (1995) High-temperature Fe–Mg cation partitioning in olivine: in situ single-crystal neutron diffraction study. Am Mineral 80: 197–200

Bhagatt SS, Bass JD, Smith JR (1992) Single-crystal elastic properties of omphacite-C2/C by Brillouin spectroscopy. J Geophys Res 97: 6843–6848

Boffa Ballaran T, Carpenter MA, Domeneghetti MC, Salje EKH, Tazzoli, V (1998) Structural mechanism of solid solution and cation ordering in augite–jadeite pyroxenes II: a microscopic perspective. Am Mineral 83: 419–433

Boffa Ballaran T, Carpenter MA, Geiger CA, Koziol AM (1999): Local structural heterogeneity in garnet solid solutions. Phys Chem Miner 26: 554–569

Boström D (1987) Single-crystal X-ray diffraction study of synthetic Ni–Mg olivine solid solutions. Am Mineral 72: 965

Cannillo E, Germani G, Mazzi F (1983) New crystallographic software for Philips PW 1100 single-crystal diffractometer. CNR centro di Studio per la Cristallografia, Internal Report

Carpenter (2003) Microscopic strain, macroscopic strain and the thermodynamic of phase transitions in minerals. In: Gramaccioli CM (ed) European notes in mineralogy, energy modelling in minerals, vol 4. European Mineralogy Union, pp 311–346

Carpenter MA, Boffa Ballaran T (2001) The influence of elastic strain heterogeneities in silicates solid solutions. In: Geiger CA (Ed), Solid solutions in silicate and oxide systems of geological importance. European notes in mineralogy, vol. 3. European Mineralogy Union, pp 155–178

Chopelas A (1991) Single-crystal spectra of forsterite, fayalite, and monticellite. Am Mineral 76: 1101–1109

Christian JW (1975) The theory of transformations in metals and alloys: An advance textbook in physical metallurgy, 2nd ed. Pergamon Press, London

Davies PK, Navrotsky A (1983) Quantitative correlations of deviations from ideality in binary and pseudobinary solid solutions. J Solid State Chem 46: 1–22

Geiger CA (2001) Thermodynamic mixing properties of binary oxide and silicate solid solution determined by direct measurement: the role of strain. In: Geiger CA (ed) Solid solutions in oxide and silicate systems. European notes in mineralogy, vol. 3. European Mineralogy Union, pp 71–100

Geiger CA, Kolesov BA (2003) Microscopic–macroscopic relationship in silicates: examples from IR and Raman spectroscopy and heat-capacity measurements. In: Gramaccioli CM (ed) Energy modelling in minerals. European notes in mineralogy, vol 4. European Mineralogy Union, pp. 1–38

Greenwood HJ (1979) Some linear and non-linear problems in petrology. Geochim Cosmochim Acta 34: 1029–1033

Hackwell TP, Angel RJ (1992) The comparative compressibility of reedmergnerite, danburite, and their aluminium analogues. Eur J Mineral 4: 1221–1227

Hofmeister (1987) Single-crystal absorption and reflection infrared spectroscopy of forsterite and fayalite. Phys Chem Miner 14: 499–513

Hofmeister AM (1997) Infrared reflectance spectra of fayalite, and absorption data from assorted olivines, including pressure and isotope effects. Phys Chem Miner 19: 460–471

Hofmeister AM, Fagan TJ, Campbell KM, Schaal RB (1996) Single-crystal IR spectroscopy of pyrope-almandine garnets with minor amounts of Mn and Ca. Am Mineral 81: 418–428

Jackson JM, Sinogeikin SV, Bass JD (1999) Elasticity of $MgSiO_3$ orthoenstatite. Am Mineral 84: 677–680

Kandelin J, Weidner DJ (1988) The single-crystal elastic properties of jadeite. Phys Earth Planet Int 50: 251–260

Kawasaki T, Matsui Y (1983) Thermodynamic analyses of equilibria involving olivine, orthopyroxene and garnet. Earth Planet Sci Lett 37: 159–166

Kojitani H and Akaogi M (1994) Calorimetric study of olivine solid solutions in the system Mg_2SiO_4–Fe_2SiO_4. Phys Chem Miner 20: 536–540

Kudoh Y, Takeuchi T (1985) The crystal structure of forsterite Mg_2SiO_4 under high pressure up to 149 kbar. Z Kristallogr 117: 292–302

Lazarev AN (1972) Vibrational spectra and structure of silicates. New York (NY) Consultants Bureau

Levien L, Prewitt CT (1981) High-pressure structural study of diopside. Am Mineral 66: 316–323

McCornick TC, Hazen RM, Angel RJ (1989) Compressibility of omphacite to 60 kbar role of vacancies. Am Mineral 74: 1287–1292

McMillan P (1985) Vibrational spectra in the mineral sciences. In: Kieffer SW, Navrotsky A (eds) Microscopic to macroscopic: atomic environments to mineral thermodynamics. Rev Mineral Geochem 14: 9–53

Newton RC, Wood BJ (1980) Volume behavior of silicate solid solutions. Am Mineral 65: 733–745

Nishihara Y, Takahashi E, Matsukage K, Kikegawa T (2003) Thermal equation of state of omphacite. Am Mineral 88: 80–86

O'Neill HSC, Wood BJ (1979) An experimental study of Fe–Mg partitioning between garnet and olivine and its calibration as a geothermometer. Contrib Mineral Petrol 70: 59–70

Redfern SAT, Artioli G, Rinaldi R, Henderson CMB, Knight KS, Wood BJ (2000) Octahedral cation ordering at high temperature. II. An in situ neutron powder diffraction study on synthetic $MgFeSiO_4$ (Fa50). Phys Chem Miner 27: 630–637

Rinaldi R, Artioli G, Wilson CC, McIntyre G (2000) Octahedral cation ordering at high temperature. I. In situ neutron single crystal studies. Phys Chem Miner 27: 623–629

Salje EKH, Carpenter MA, Malcherek T, Boffa Ballaran T (2000) Autocorrelation analysis of infrared spectra from minerals. Eur J Mineral 12: 503–519

Schwab RG, Küstner D (1977) Präzisionsgitterkonstantenbestimmung zur Festlegung röntgenographischer Bestimmungkurven für synthetische Olivine der Mischkristallreihe Forsterit-Fayalit. N Jb Miner Mh 205–215

von Seckendorff V, O'Neill HSC (1993) An experimental study of Fe–Mg partitioning between olivine and orthopyroxene at 1173 K and 1423 K and 1.6 GPa. Contrib Mineral Petrol 113: $196–207_{22}$

Tarantino SC, Boffa Ballaran T, Carpenter MA, Domeneghetti MA, Tazzoli V (2002) Mixing properties of the enstatite–ferrosilite solid solution: II A microscopic perspective. Eur J Mineral 14: 537–547

Wiser NM, Wood BJ (1991) Experimental determination of activities in Fe–Mg olivine at 1400 K. Contrib Mineral Petrol 108: 146–153

Wood BJ, Kleppa OJ (1981) Thermochemistry of forsterite–fayalite olivine solid solutions Geochim Cosmochim Acta 45: 529–534

Zhao Y, Von Dreele RB, Shankland TJ, Weidner DJ, Zhang J, Wang Y, Gasparik T (1997) Thermoelastic equation of state of jadeite $NaAlSi_2O_6$: an energy-dispersive Rietvield refinement study of low symmetry and multiple phases diffraction. Geophys, Reserch Lett

Zhao Y, Von Dreele RB, Zhang J, Weidner (1998) Thermoelastic equation of state of monoclinic pyroxene $CaMgSi_2O_6$: diopside. Rev High- Press Sci Technol 7: 25–27

Zhang M, Wruck B, Graeme-Barber A, Salje EKH, Carpenter MA (1996) Phonon spectroscopy on alkali-feldspars: phase transitions and solid solutions. Am Mineral 81: 92–104